Rock physics models for cracked media

Zimin Zhang and Robert R. Stewart

ABSTRACT

Two rock physics models for cracked media are investigated in this paper: the Kuster-Toksöz model for randomly oriented cracks and Hudson's model for aligned cracks. The effects of crack shape, aspect ratio and crack density are discussed using rock properties from several field locations: the Ross Lake heavy oil field, Saskatchewan; Violet Grove Alberta CO_2 injection site; and a Saskatchewan mining area.

Inclusion shape has a large influence on the effective rock properties from the Kuster-Toksöz model. Generally, smaller aspect ratios (thinner cracks) yield larger drops of moduli and velocities. Through the modeling results for the rocks from the chosen areas, 1% porosity by penny shape cracks with aspect ratio 0.01 can produce up to 22% velocity decreases from Hudson's model, and 16% P-velocity and 11% S-velocity drops from Kuster-Toksöz model. The results also indicate: the percentage changes of S-velocity from both models and P-velocity along crack planes from Hudson's method have almost no dependence on uncracked rock properties; while the percentage changes of P-velocity (P-velocity along crack normal for Hudson's model results) are consistent with the values of uncracked rocks for Kuster-Toksöz model and Hudson's method without fluid substitution; and anisotropic fluid substitution introduces higher percentage of P-velocity changes and similar S-velocity changes.

INTRODUCTION

The Kuster and Toksöz (1974) method (Appendix 1) calculates the effective moduli for randomly distributed inclusions based on a long-wavelength, first-order scattering theory. The overall effect of the inclusions is isotropic. The Hudson (1981) model (Appendix 2) is based on a scattering theory analysis of the mean wave field in an elastic solid with thin, penny-shaped ellipsoidal cracks or inclusions which are aligned with a specific direction. The effective moduli can be calculated by applying the first- and second- order corrections on the isotropic background moduli. The overall effect of the aligned cracks is anisotropic.

Both models assume no fluid flow between spaces, thus they simulate high-frequency, saturated rock behavior. At low frequencies, when there is time for wave-induced pore pressure increments to flow and equilibrate, Gassmann fluid substitution (Mavko et. Al., 1998) for isotropic media and Brown and Korringa's (1975) fluid substitution for anisotropic media are necessary to predict saturated rock properties.

In this paper, the effects of crack shape, aspect ratio and crack density will be discussed. Some parameters for crack description are given in Appendix 3.

Rock properties for numerical test

Several rock types are selected to provide numerical test and examples: a Cretaceous-aged, high-porosity (about 30%) channel sand and a tight sand from the Ross Lake heavy

oil field, another Cretaceous-aged low-porosity (about 12%) sandstone from Violet Grove, Alberta, and a Devonian carbonate and a shale from a potash mining area in Saskatchewan. The rock properties for these rocks are listed in Table 1. The porous channel sand and tight sand from Ross Lake area were used for various parameter tests with the Kuster-Toksöz model and Hudson's model. Then cracked rock properties are calculated for all the chosen rocks assuming penny cracks with a fractional crack porosity 0.01 and aspect ratio 0.01. For all the tests, the void spaces are filled by brine water, at a density of 1.1g/cm^3 and velocity of 1430m/s.

Table 1. Rock properties for numerical test for models of cracked media

	Ross Lake		Violet Grove	Sask. mining	
Lithology	Sandstone	Sandstone	Sandstone	Carbonate	shale
Depth	1148m	1160m	1605m	970m	1006m
Vp (m/s)	3026	5689	3778	5538	3765
Vs (m/s)	1721	3413	2237	2954	2074
Density (g/cc)	2.133	2.63	2.42	2.695	2.326
Porosity	30%	2%	12%	3%	<5%

Hashin-Shtrikman bound

When the geometries of each constituent in the rock are unknown, the upper and lower bounds of effective moduli of the rock can be estimated, given the volume fraction and moduli of each constituent. When only the volume fraction and elastic moduli are given for each component of the rock, Hashin-Shtrikman bound (Mavko et. Al., 1998) was the narrowest bound without knowing the geometries of the constituents. They were used to validate the modeling results. The equations can be written as:

$$K^{HS\pm} = K_1 + \frac{f_2}{(K_2 - K_1)^{-1} + f_1\left(K_1 + \frac{4}{3}\mu_1\right)^{-1}}, \quad 1)$$

$$\mu^{HS\pm} = \mu_1 + \frac{f_2}{(\mu_2 - \mu_1)^{-1} + \frac{2f_1(K_1 + 2\mu_1)}{5\mu_1\left(K_1 + \frac{4}{3}\mu_1\right)}}, \quad 2)$$

where

- K_1, K_2 : bulk moduli of individual component;
- μ_1, μ_2 : shear moduli of individual component;
- f_1, f_2 : volume fractions of individual component.

By interchanging component 1 and 2 in the formula, the upper and lower bounds are calculated. When the stiffest material is termed 1, the upper bound will be given; otherwise, when the softest phase is termed 1, the lower bound will be calculated.

KUSTER-TOKSÖZ MODEL

Figure 1a, 2 display the results of randomly oriented inclusions in the porous channel sand in Ross Lake Heavy Oil Field as calculated by the Kuster-Toksöz model. Dry moduli were calculated first supposing both bulk and shear modulus of the inclusions to be 0, then the Gassmann equation was used to calculate the effective moduli when the void space is filled by brine. From Figure 1a, we find that the rock properties largely depend on the inclusion shape. For fluid phase constituent, the disk shape of Kuster-Toksöz model does not converge. For other inclusion shapes, smaller aspect ratios yield a larger decrease of moduli and velocities. For both dry and saturated rock, the moduli and velocities of sphere inclusion shape are coincident with Hashin-Shtrikman upper bound. The sphere inclusion shapes give the same results from the Kuster-Toksöz (1974) formula and generalized formula (Berryman, 1980). The effective bulk modulus of small aspect ratio inclusion shape approaches Hashin-Shtrikman lower bound at smaller volume fraction of pores. Except for the sphere shape inclusion, all other inclusion shapes have a limitation on volume fraction values for reasonable effective moduli values. The concentration value limitations decrease with aspect ratio. For needle shape inclusions, it does not depend on aspect ratio. It is valid for large range of concentration values, approximately up to 0.8.

The same calculation was also carried out for tight sand of Ross Lake Heavy Oil Field (Figure 1b), it gives very close result. The concentration limitations for each inclusion shape are quite similar to those of the porous sand.

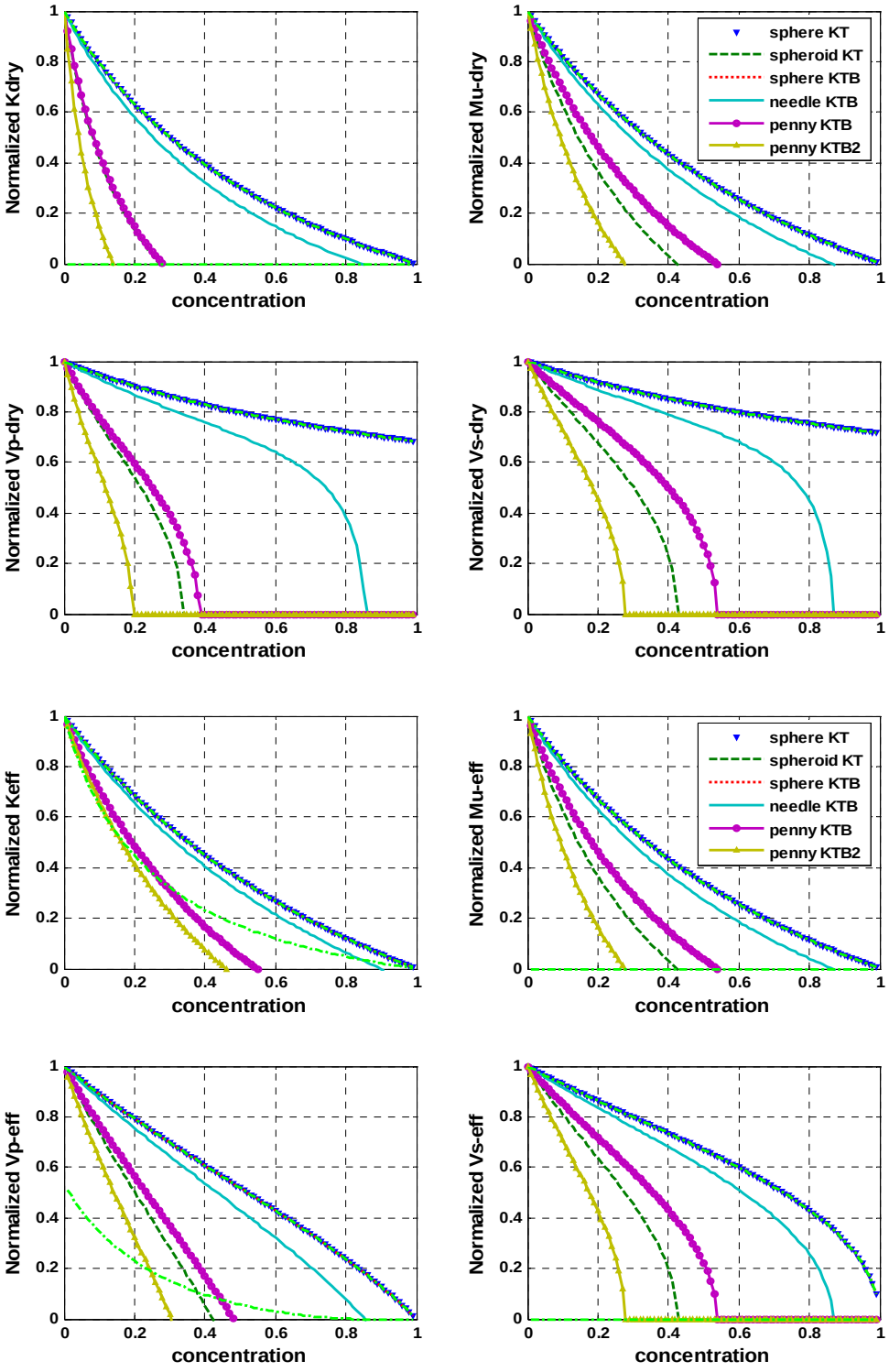

FIG. 1a. Ross Lake porous channel sand: variation of effective dry and saturated rock properties for several crack shapes from Kuster-Toksöz model with volume concentration of inclusion. All the elastic property values are normalized to the range from fluid to uncracked rock properties. The aspect ratio value for oblate spheroid shape is 0.1. For penny shape, aspect ratio 0.1 (noted as penny KTB) and 0.05 (noted as penny KTB2) are used. KT: the results from Kuster-Toksöz formula for sphere and oblate spheroid shape inclusions, KTB: the results from generalized Kuster-Toksöz model by Berryman. The green dash-dot lines are Hashin-Shtrikman bounds.

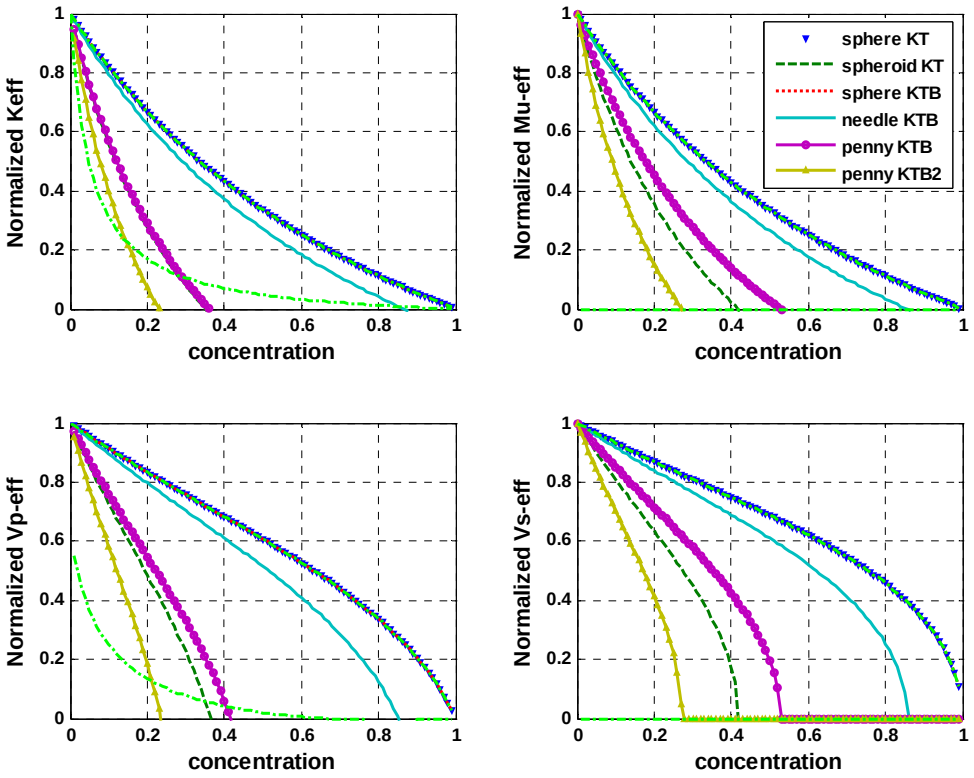

FIG. 1b. Ross Lake tight sand: variation of effective dry and saturated rock properties for several crack shapes from Kuster-Toksöz model with volume concentration of inclusion. All the elastic property values are normalized to the range from fluid to uncracked rock properties. The aspect ratio value for oblate spheroid shape is 0.1. For penny shape, aspect ratio 0.1 (noted as penny KTB) and 0.05 (noted as penny KTB2) are used. KT: the results from Kuster-Toksöz formula for sphere and oblate spheroid shape inclusions, KTB: the results from generalized Kuster-Toksöz model by Berryman. The green dash-dot lines are Hashin-Shtrikman bounds.

From the formula of Kuster-Toksöz-Berryman model (Appendix 1), we know that only spheroid and penny shape related to aspect ratio α. Figure 2 shows the variation of effective moduli with aspect ratio α for spheroid and penny shape pore. The volume fraction c of pore was set to be 0.1. When aspect ratio is too small (approximately $\alpha/c<0.4$), the assumption of no fluid flow cannot be satisfied, thus the model can't give reasonable results. When aspect ratio increases, the moduli drops will decrease. The results of spheroid shape will approach those of sphere shape. For penny shape, the aspect ratio can not be too large (α/c value depends on the volume fraction of the penny pores, the larger volume fraction, the less tolerance is for big aspect ratio), otherwise, the predicted moduli will exceed the upper bound of the effective moduli.

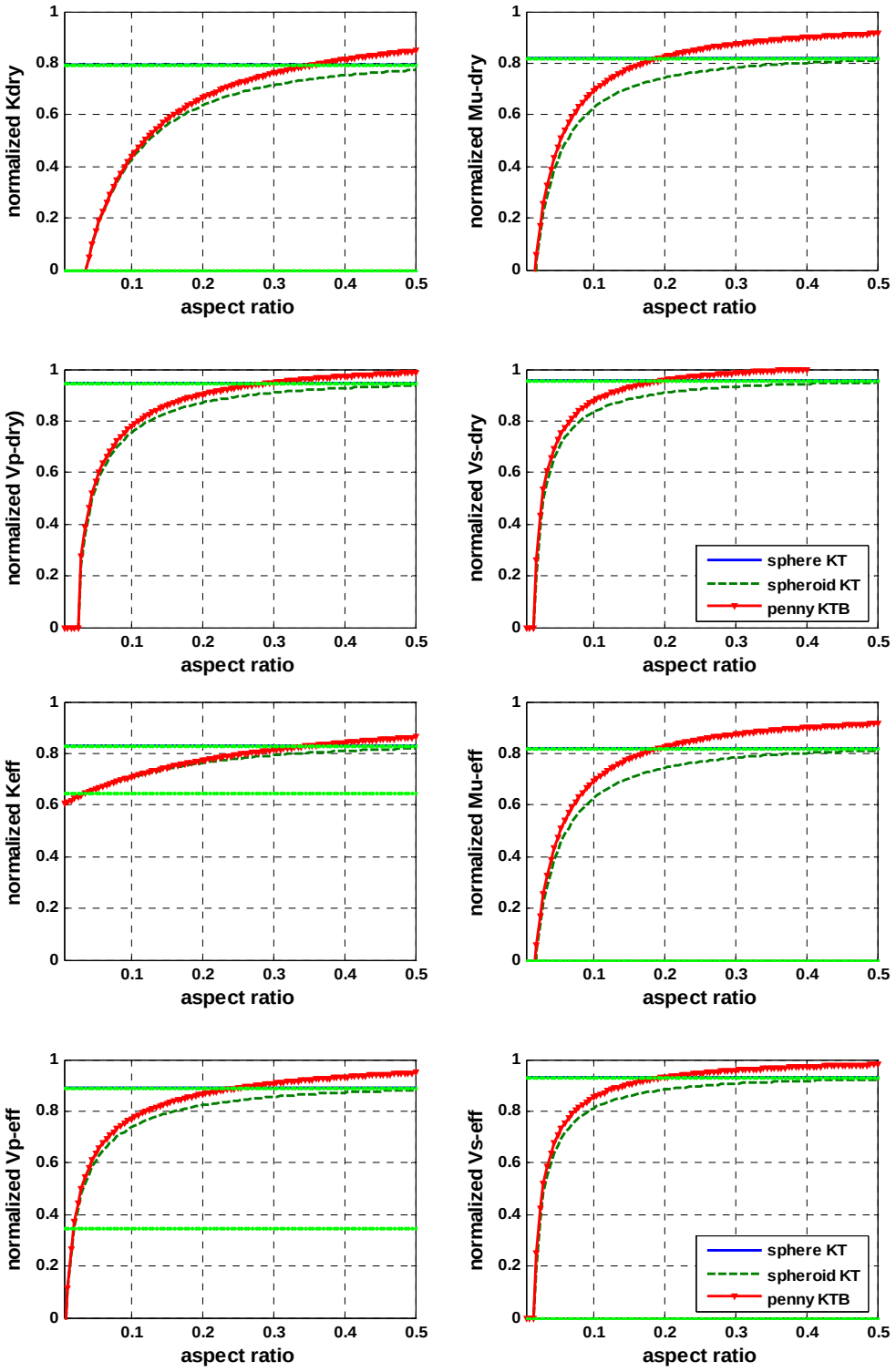

FIG. 2. Ross Lake porous channel sand: variation of dry and saturated effective rock properties from Kuster-Toksöz model with crack shape and aspect ratio. All the values are normalized to the range from saturated fluid to unaltered rock properties. The volume fraction of crack c is 0.1. The green dash-dot lines are Hashin-Shtrikman bounds. KT: results from Kuster-Toksöz formula; KTB: results from generalized Kuster-Toksöz model by Berryman.

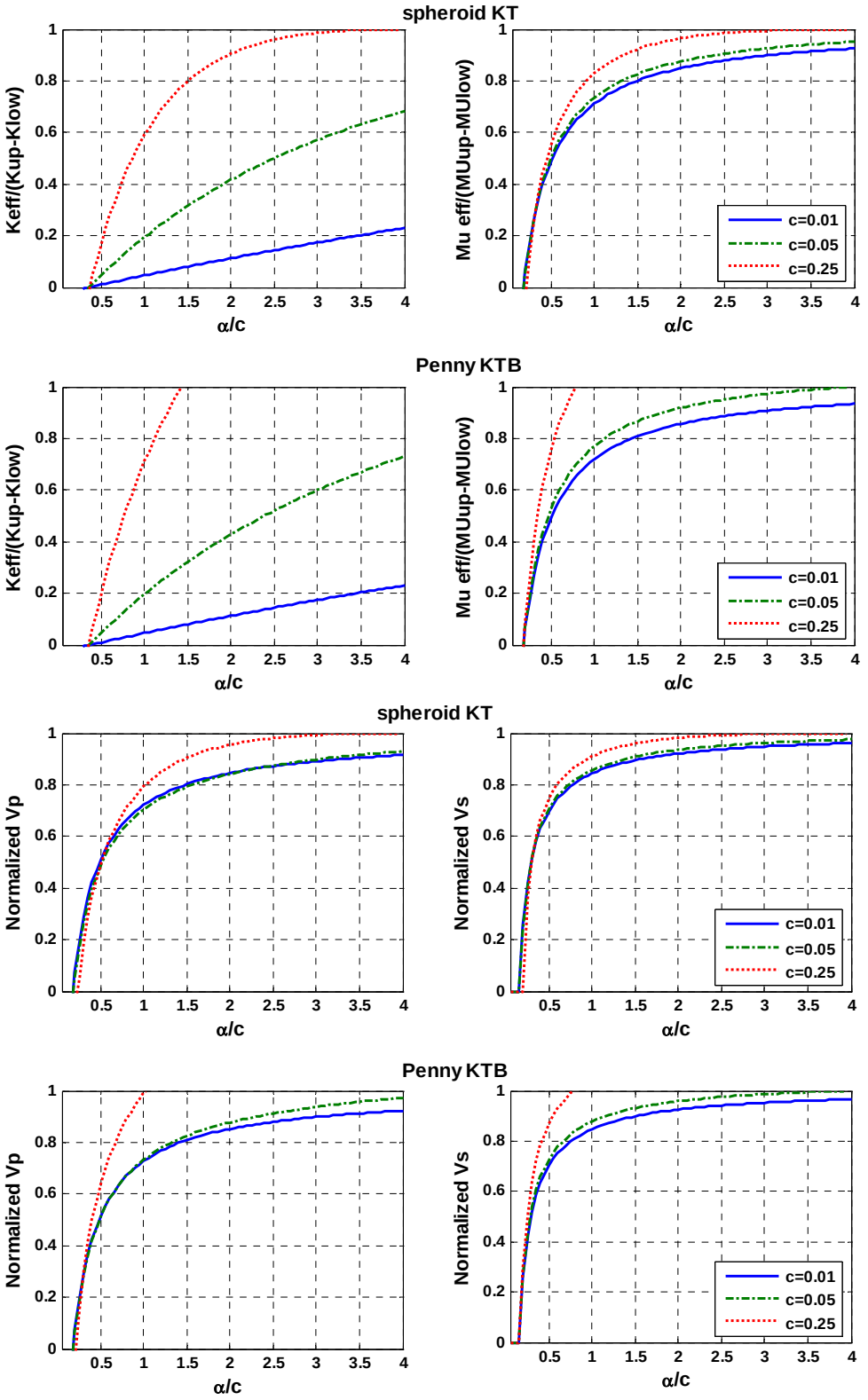

FIG. 3a. Ross Lake porous channel sand: variation of effective rock properties from Kuster-Toksöz model with α/c value (aspect ratio/volume concentration). All the values are normalized to the range of Hashin-Shtrikman bounds.

From the result displayed in Figure 2, α/c value should be within some range so that the predicted moduli fall within the Hashin-Shtrikman bound. To investigate the value range, a test on α/c value with different c values (0.01, 0.05, and 0.25) was carried out and the results are shown in Figure 3a. The moduli and velocity values in Figure 3a were normalized by Hashin-Shtrikman upper and lower bound. For various c values, both bulk modulus and shear modulus indicate relatively stable minimum α/c values, approximated 0.4 for bulk modulus and 0.2 for shear modulus. However, for penny shape inclusion, the maximum α/c values for reasonable moduli change drastically with respect to crack concentration value c. Small c values will still have reasonable effective moduli for large α/c value. Besides, compared with shear moduli, the bulk moduli have less limitation on α/c value. For spheroid shape inclusions, there is no upper limitation of α/c value, but with increasing c value, the moduli approach upper bound quickly. From the velocities changes, we find the effects of c value are less than that on moduli. And the minimum α/c values are very similar to P- and S-velocities, about 0.2. From the similar calculation carried out on tight sand of Ross Lake Heavy Oil Field (Figure 3b), a similar conclusion can be made.

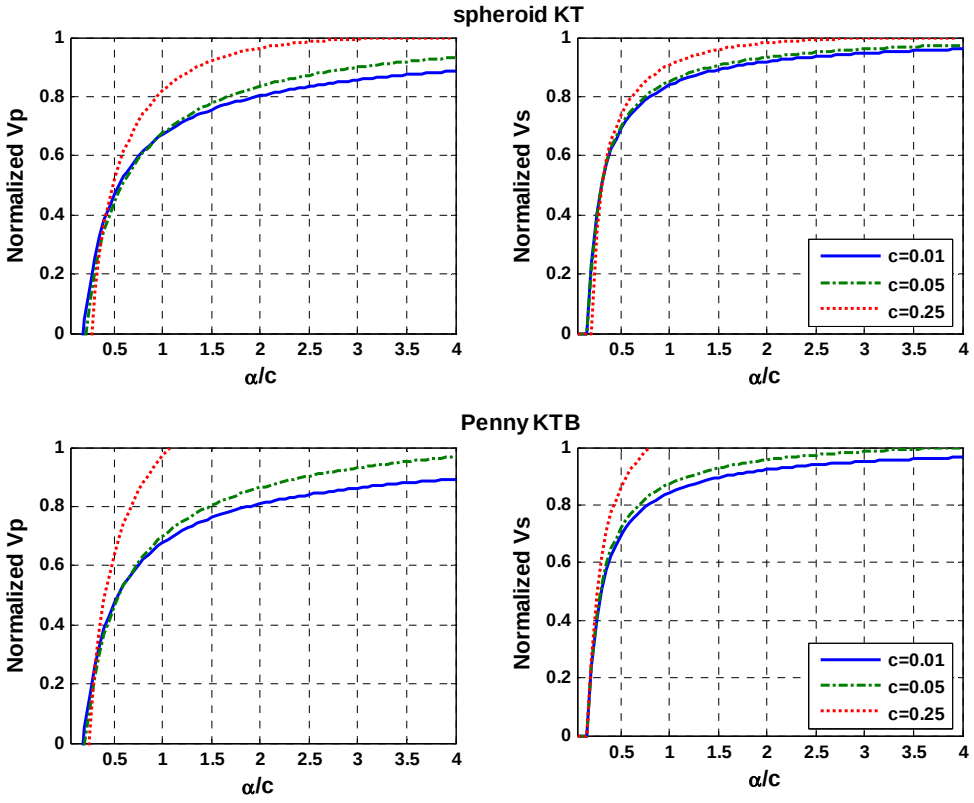

FIG. 3b. Ross Lake tight sand: variation of effective velocities from Kuster-Toksöz model with α/c value (aspect ratio/volume concentration). All the values are normalized to the range of Hashin-Shtrikman bounds.

HUDSON'S MODEL

Figure 4a show the results of Ross Lake porous channel sand from Hudson's model for penny cracks with three aspect ratios (α): 0.002, 0.01, and 0.05. It displays the modeled P- and S-velocity variation with crack density. When the rock contains aligned

cracks, it will display anisotropy. For the cracks are aligned for one direction, it will show transverse anisotropy with respect to the axis along crack normal. The P-velocity drops very little when the waves travel along crack plane, but it will display distinct decrease when the wave travels along crack normal. For SV wave, the velocity will change the same amount whether it travels along the crack normal or crack plane. Cracks with aspect ratio 0.05 are also modeled by Kuster-Toksöz-Berryman penny crack model, the effective P-velocities from Kuster-Toksöz model is between the P-velocities from Hudson's model along crack normal and crack plane.

We also find that small aspect ratio cracks have very limited crack density range, especially for Vs, approximate 0.05 (about crack porosity 0.1% equivalent) for cracks with aspect ratio 0.002 and 0.2 (equivalent to about 1% crack porosity) for cracks with aspect ratio 0.01. When crack density value is greater than the limitation, the velocity will display abnormal increase with increasing porosity.

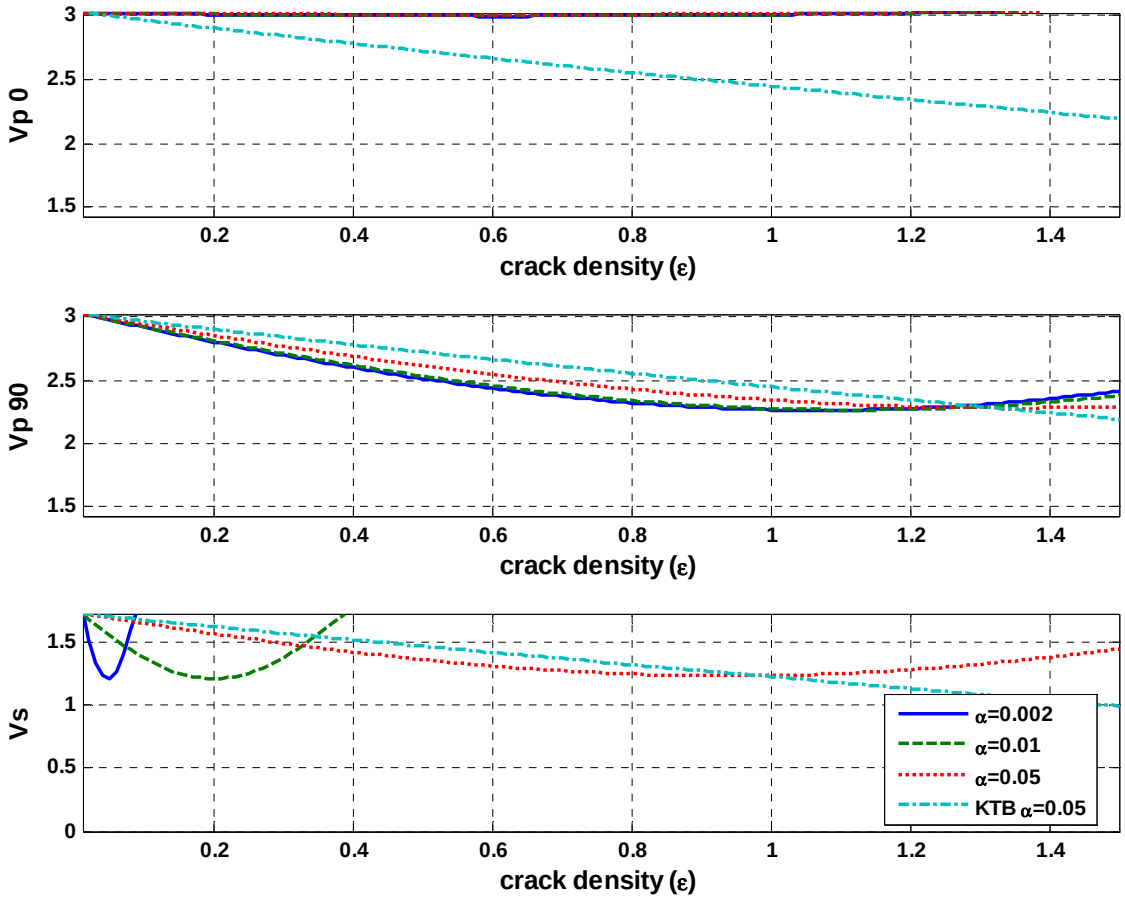

FIG. 4a. Ross Lake porous channel sand: variation of effective velocities of cracked rock from Hudson's model with crack density. The maximum and minimum velocity values in the plot are those of isotropic uncracked rock and saturated fluid respectively. KTB denotes the effective velocities from Kuster- Toksöz model.

From the modeling results for tight sand from Ross Lake area (Figure 4b), we found that the P-velocity variations with crack density show apparent dependence on rock

properties of the uncracked rock. While the S-velocity displays quite similar variation with crack density. However, the reasonable crack density ranges for each aspect ratio are still the same due to the similar variation of S-velocity with crack density.

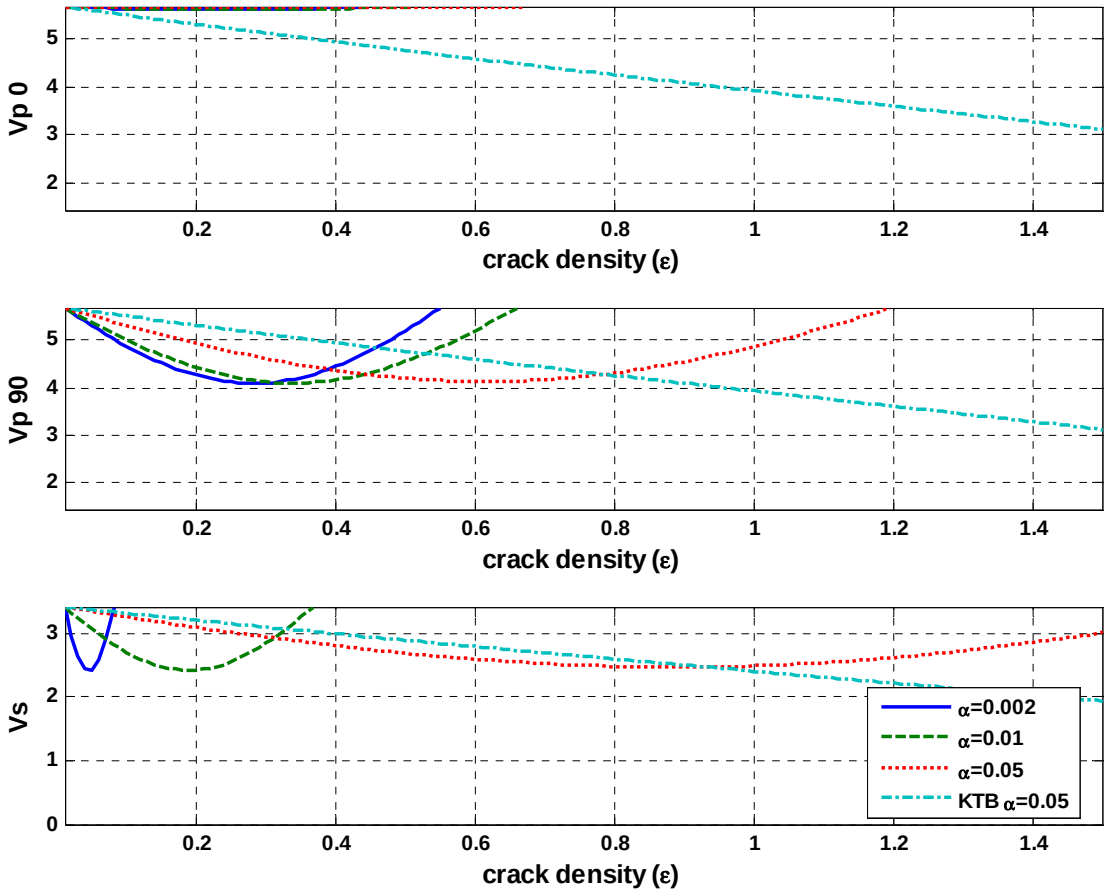

FIG. 4b. Ross Lake tight sand: variation of effective velocities of cracked rock from Hudson's model with crack density. The maximum and minimum velocity values in the plot are those of isotropic uncracked rock and saturated fluid respectively. KTB denotes the effective velocities from Kuster- Toksöz model.

Assuming 1% crack porosity introduced by penny shape cracks with aspect ratio 0.01, the effective P- and S-velocities from Kuster-Toksöz and Hudson's model are listed in Table 2 and plotted in Figure 5 for variant lithology rocks from several chosen areas across Western Canada Sedimentary Basin. From the results, we find:

1. The percentage changes of S-velocity induced by the cracks are quite similar for each rock from both models;

2. The percentage changes of P-velocity along crack planes are very similar from Hudson's method without or with fluid substitution;

3. The percentage changes of P-velocity (P-velocity along crack normal for Hudson's model results) are consistent with the values of uncracked rocks from Kuster-Toksöz model and Hudson's method without fluid substitution;

4. Anisotropic fluid substitution introduces higher percentage of P-velocity changes and similar S-velocity changes.

Table 2. Modeled effective rock properties for selected reservoir rocks assuming penny shape cracks with aspect ratio 0.01, crack density 0.01 in the rock. %: velocity change percentage with respect to original velocity; Vp0: P-velocity along the crack plane; Vp90: P-velocity along crack normal; Vsv: S-velocity along the crack plane.

			Ross Lake		Violet Grove	Sask. mining	
Lithology			Sandstone	Sandstone	Sandstone	Carbonate	Shale
Depth			1148m	1160m	1605m	970m	1006m
Raw		Vp (m/s)	3026	5689	3778	5538	3765
		Vs(m/s)	1721	3413	2237	2954	2074
		Density (g/cc)	2.13	2.63	2.42	2.695	2.326
Kuster- Toksöz		Vp(m/s)	2800	5047	3442	4944	3464
		%	7.5	11.3	8.9	10.8	8
		Vs(m/s)	1449	2856	1875	2505	1753
		%	15.8	16.3	16.2	15.2	15.5
Hudson	No fluid substitution	Vp0(m/s)	3019	5649	3767	5425	3739
		%	0.3	0.7	0.3	2	0.7
		Vp90(m/s)	2912	4934	3537	4819	3534
		%	3.8	13.3	6.4	13	6.1
		Vsv(m/s)	1338	2643	1734	2308	1616
		%	22.3	22.6	22.5	21.9	22.1
	Fluid substitution	Vp0(m/s)	2971	5613	3721	5461	3698
		%	1.8	1.3	1.5	1.4	1.8
		Vp90(m/s)	2497	4398	2964	5034	3253
		%	17.5	22.7	21.6	9.1	13.6
		Vsv(m/s)	1348	2696	1762	2311	1622
		%	21.7	21	21.3	21.8	21.8

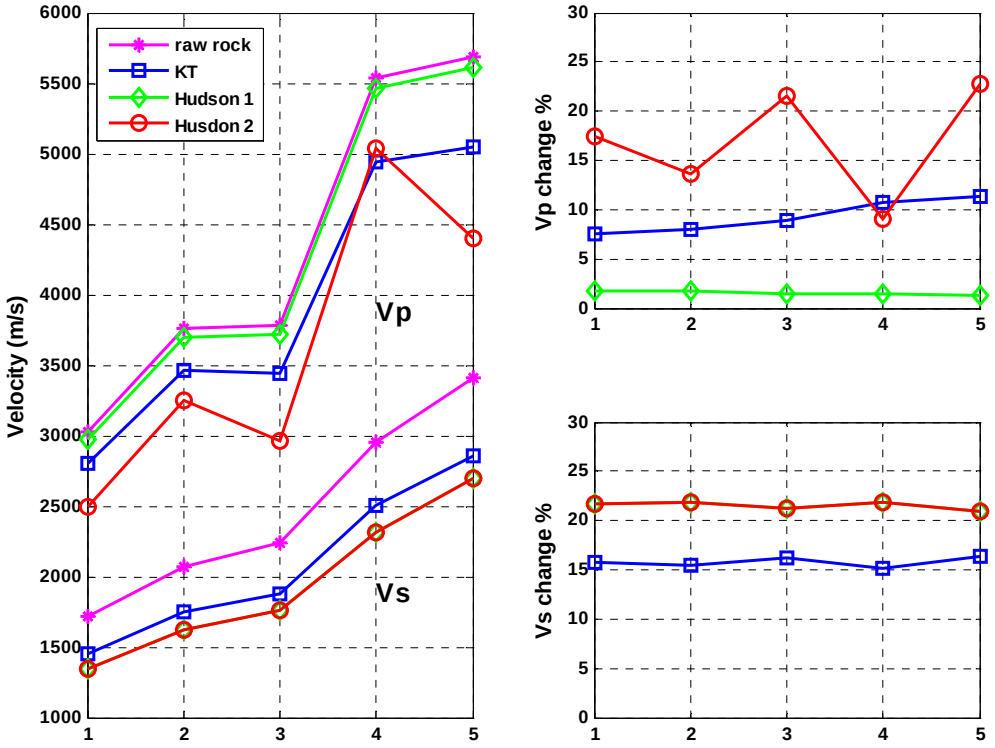

FIG. 5. Modeled effective velocities for selected reservoir rocks assuming penny shape cracks with aspect ratio 0.01, crack density 0.01 in the rock. KT: velocities from Kuster-Toksöz model. Hudson 1: P-velocity along the crack plane; Hudson 2: P-velocity along crack normal. The plots in the right are percentage changes with respect to original velocity.

CONCLUSIONS

Two rock physics models (Kuster-Toksöz and Hudson) for cracked media are discussed. With given assumptions, the Kuster-Toksöz and the Hudson's methods can predict rock properties within Hashin-Shtrikman bounds for randomly oriented cracks and aligned cracks respectively.

From the results of Kuster-Toksöz model, we found the rock properties largely depend on the inclusion shape. Generally, the smaller aspect ratios yield a larger decrease of moduli and velocities. For both spheroid and penny shape inclusions, α/c values should not be smaller than about 0.4 (equivalent to $c<2.5\alpha$). As for penny shape inclusions, the valid maximum α/c values change drastically with respect to concentration value c. Small c values will still have reasonable effective moduli for large α/c value.

For Hudson's model, smaller aspect ratio cracks have smaller valid crack density range, especially for Vs, approximate 0.05 (about crack porosity 0.1% equivalent) for cracks with aspect ratio 0.002 and 0.2 (equivalent to about 1% crack porosity) for cracks with aspect ratio 0.01.

The modeling results for several rocks assuming 1% crack porosity, 0.01 aspect ratio penny shape cracks indicate: the percentage changes of S-velocity from both models and P-velocity along crack planes from Hudson's method have almost no dependence on

uncracked rock properties; while the percentage changes of P-velocity (P-velocity along crack normal for Hudson's model results) are consistent with the values of uncracked rocks for Kuster-Toksöz model and Hudson's method without fluid substitution; anisotropic fluid substitution introduces higher percentage of P-velocity changes and similar S-velocity changes.

ACKNOWLEDGEMENTS

The authors gratefully acknowledge the support of CREWES sponsors.

REFERENCE

Berryman, J.G., 1980, Long-wavelength propagation in composite elastic media: J. Acoust. Soc. Am., **68**, 1809-1831.

Brown, R., and Korringa, J., 1975, On the dependence of the elastic properties of a porous rock on the compressibility of the pore fluid: Geophysics, **40**, 606-616.

Chen, F., 2006, Interpretation of Time-lapse Surface Seismic Data at a CO_2 Injection Site, Violet Grove, Alberta: M.Sc. Thesis, Univ. of Calgary.

Hudson, J.A., 1981, Wave speeds and attenuation of elastic waves in material containing cracks: Geophys. J. Royal Astronom. Soc. **64**, 133-150.

Kuster, G.T., and Toksöz, M.N., 1974, Velocity and attenuation of seismic waves in two-phase media: Part I. theoretical formulations: Geophysics, **39**, 587-606.

Mavko, G., Mukerji, T., and Dvorkin, J., 1998, The rock physics handbook: Cambridge University Press.

APPENDIX 1: KUSTER-TOKSÖZ MODEL

Based on a long-wavelength first-order scattering theory, Kuster and Toksöz (1974) derived a method to calculate effective moduli for randomly distributed inclusions. A generalization of the expressions for the effective moduli K^* and μ^* can be written as (Kuster and Toksöz, 1974; Berryman, 1980),

$$(K_m - K^*)\frac{K_m+\frac{4}{3}\mu_m}{K^*+\frac{4}{3}\mu_m} = \sum_{i=2}^{N} c_i(K_m - K_i)P^{mi}, \quad \text{(A1)}$$

$$(\mu_m - \mu^*)\frac{\mu_m+F_m}{\mu^*+F_m} = \sum_{i=2}^{N} c_i(\mu_m - \mu_i)Q^{mi}, \quad \text{(A2)}$$

and

$$\rho_1 - \rho^* = \sum_{i=2}^{N} c_i(\rho_1 - \rho_i), \quad \text{(A3)}$$

where,

- $c_i = \Omega_i/\Omega$ is volume concentration of each inclusion types and $\sum_{i=1}^{N} c_i = 1$, Ω: volume;
- K_i, μ_i: moduli of inclusion;
- K_m, μ_m: moduli of matrix;
- $F_m = (\mu_m/6)[(9K_m + 8\mu_m)/(K_m + 2\mu_m)]$;
- P^{mi}, Q^{mi}: coefficients describing the effect of an inclusion of material *i* in a background medium m (Table A1);
- ρ_1, ρ_i, ρ^*: density of matrix, inclusion and effective density.

Table A1. Coefficients P^{mi} and Q^{mi} for four types of inclusion. Where, $F = (\mu/6)[(9K + 8\mu)/(K + 2\mu)]$, $\gamma = \mu[(3K + \mu)/(3K + 7\mu)]$, $\beta = \mu[(3K + \mu/(3K + 4\mu))]$, and the aspect ratio α. The expressions for spheres, needles, and disks were derived assuming $K_i/K_m \ll 1$ and $\mu_i/\mu_m \ll 1$.

Inclusion shape	P^{mi}	Q^{mi}
Spheres	$\frac{K_m+\frac{4}{3}\mu_m}{K_i+\frac{4}{3}\mu_m}$	$\frac{\mu_m+F_m}{\mu_i+F_m}$
Needles	$\frac{K_m+\mu_m+\frac{1}{3}\mu_i}{K_i+\mu_m+\frac{1}{3}\mu_i}$	$\frac{1}{5}\left(\frac{4\mu_m}{\mu_m+\mu_i}+2\frac{\mu_m+\gamma_m}{\mu_i+\gamma_m}+\frac{K_i+\frac{4}{3}\mu_m}{K_i+\mu_m+\frac{1}{3}\mu_i}\right)$
Disks	$\frac{K_m+\frac{4}{3}\mu_m}{K_i+\frac{4}{3}\mu_m}$	$\frac{\mu_m+F_i}{\mu_i+F_i}$
Penny cracks	$\frac{K_m+\frac{4}{3}\mu_i}{K_i+\frac{1}{3}\mu_i+\pi\alpha\beta_m}$	$\frac{1}{5}\left(1+\frac{8\mu_m}{4\mu_i+\pi\alpha(\mu_m+2\beta_m}+2\frac{K_i+\frac{2}{3}\mu_i+\frac{2}{3}\mu_m}{K_i+\frac{4}{3}\mu_i+\pi\alpha\beta_m}\right)$

APPENDIX 2: HUDSON'S MODEL

The Hudson (1981) model is based on a scattering theory analysis of the mean wave field in an elastic solid with thin, penny-shaped ellipsoidal cracks or inclusions. The effective moduli,

$$c_{ij}^{eff} = c_{ij}^{0} + c_{ij}^{1} + c_{ij}^{2}, \qquad \text{(A4)}$$

where c_{ij}^{0} are the isotropic background moduli, and c_{ij}^{1}, c_{ij}^{2} are the first- and second-order corrections, respectively.

For a single crack set with crack normal aligned with the 3rd axis (Figure A1), the cracked media show transverse isotropic symmetry, and the corrections are

- $c_{11}^{1} = -\frac{\lambda^2}{\mu}\varepsilon U_3$
- $c_{13}^{1} = -\frac{\lambda(\lambda+2\mu)}{\mu}\varepsilon U_3$
- $c_{33}^{1} = -\frac{(\lambda+2\mu)^2}{\mu}\varepsilon U_3$
- $c_{44}^{1} = -\mu\varepsilon U_1$
- $c_{66}^{1} = 0$

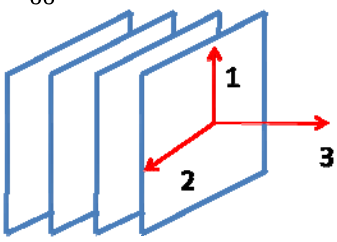

FIG. A1. Schematic diagrams of aligned cracks (shown in blue).

$$U_1 = \frac{16(\lambda+2\mu)}{3(3\lambda+4\mu)}\frac{1}{(1+M)}, \qquad U_3 = \frac{4(\lambda+2\mu)}{3(\lambda+\mu)}\frac{1}{(1+\kappa)}$$

where

$$M = \frac{4\mu'}{\pi\alpha\mu}\frac{(\lambda+2\mu)}{(3\lambda+4\mu)}, \qquad \kappa = \frac{[K'+(\frac{4}{3})\mu'](\lambda+2\mu)}{\pi\alpha\mu(3\lambda+4\mu)}$$

K' and μ' are the bulk and shear modulus of the inclusion material. The criteria for an inclusion to be "weak" depend on its shape or aspect ratio α as well as on the relative moduli of the inclusion and matrix material. Dry cavities can be modeled be setting the inclusion moduli to zero. Fluid-saturated cavities are simulated by setting the inclusion shear modulus to zero.

APPENDIX 3: CRACK DESCRIPTION

There are several parameters often used to describe simplified versions of a cracked rock:

The quantity α=b/c is called the aspect ratio.

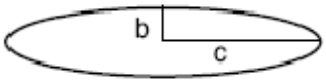

The crack density is the number of cracks per unit volume: $\varepsilon = \frac{Nc^3}{V_{bulk}}$

where,

N: number of cracks in volume Vbulk;

c: semi-major axis value of cracks.

If we assume a rock contains N/V_b thin oblate spheroidal cracks per unit bulk volume, each having semi-major axis and semi-minor axis b=αc, where α is the aspect ratio, the *crack porosity* will be:

$$\phi = \frac{N}{V_b}\frac{4\pi c^2 b}{3} = \frac{N}{V_b}\frac{4\pi c^3 \alpha}{3}$$

Where *N* is the number of cracks in volume V_b; *c*: semi-major axis value of cracks; α: aspect ratio.

Thus, crack density is:

$$\epsilon = \frac{N}{V}c^3 = \frac{3\phi}{4\pi\alpha}$$